Carbon 167 (2020) 388–402

Contents lists available at ScienceDirect

Carbon

journal homepage: www.elsevier.com/locate/carbon

Oxidation and nitridation of vitreous carbon at high temperatures

Vanessa J. Murray [a], Pedro Recio [b], Adriana Caracciolo [b], Chloe Miossec [b], Nadia Balucani [b], Piergiorgio Casavecchia [b], Timothy K. Minton [a, *]

[a] Department of Chemistry and Biochemistry, Montana State University, 103 Chem/Biochem Bldg, Bozeman, MT 59717, United States
[b] Dipartimento di Chimica, Biologia e Biotecnologie Universita, Degli Studi di Perugia, 06123, Perugia, Italy

ARTICLE INFO

Article history:
Received 20 April 2020
Received in revised form
23 May 2020
Accepted 25 May 2020
Available online 27 May 2020

Keywords:
Carbon oxidation
Carbon nitridation
Hypersonic ablation
Gas-surface interactions

ABSTRACT

Molecular beam-surface scattering experiments were used to obtain fundamental data on gas-surface interactions that are central to the ablation of carbon during hypersonic flight through air. Continuous beams containing O or N atoms with incident velocities of ~2000 m s^{-1} were directed at a vitreous carbon surface at temperatures in the range, 800–1873 K, and the products that desorbed from the surface were detected with a rotatable mass spectrometer detector as a function of their velocity and scattering angle. All products exhibited the dynamical characteristics of thermal desorption. The efficiencies of the gas-surface interactions, both reactive and non-reactive, were quantified as a function of surface temperature. In addition to reacting with carbon to produce CO_2 (minor product) and CO (major product), oxygen atoms may recombine on the surface to produce O_2 with an efficiency that is somewhat lower than that to produce CO. Nitrogen atoms may recombine on the surface to produce N_2 or react to produce CN. The recombination efficiency of N atoms is generally more than an order of magnitude higher than the reaction efficiency to produce CN. The quantitative reaction efficiencies reported here are useful for the development of air-carbon models for hypersonic ablation.

1. Introduction

Understanding the oxidation and nitridation mechanisms of carbon is key to the reliable design of carbon-based heat-shield materials for hypersonic flight through air [1–4]. We have thus used molecular beam-surface scattering experiments to add new insight to our understanding of high temperature oxidation [5,6] and nitridation [7] of model carbon materials. From the individual chemical mechanisms that have been determined for atomic-oxygen interactions with carbon and from inferred reaction efficiencies, oxygen-carbon ablation models have been developed that are not tied to a specific test environment [8–10].

While the earlier molecular beam experiments provided a wealth of information on the details of the reactive and non-reactive scattering dynamics when O or N atoms strike a high-temperature carbon surface, these earlier experiments used pulsed beams of hyperthermal atoms with relatively low average fluxes. In a hypersonic boundary layer, the gas temperature may be 5000–10,000 K [11,12], leading to average atom-surface impact energies, $\langle E_i \rangle$ (where $\langle E_i \rangle = 2RT$), of ~0.85–~1.7 eV. These energies are small compared to the translational energies of the incident atoms in the earlier molecular beam studies, where $\langle E_i \rangle \approx 4.8$ eV [5–7]. Significantly higher incident energies may lead to non-thermal gas-surface interactions, such as direct inelastic scattering and Eley-Rideal or hot-atom reactions, as were observed in the earlier studies [6]. Eley-Rideal recombination of O atoms (to make O_2) or N atoms (to make N_2) is expected to be more probable with higher incident energies. The possibility that sources of the observed diatomic species could be from the incident beam or from Eley-Rideal or Langmuir-Hinshelwood recombination, as well as the uncertain angular distributions of products that scatter via non-thermal pathways (*vide infra*), made it impossible to identify O- or N-atom recombination mechanisms in the earlier studies, so these mechanisms were given little weight in the ablation models that were developed. Despite the presence of non-thermal interactions, the earlier studies showed that thermal processes dominated, especially in the reactions that removed carbon from the surface, and the thermal processes were assumed to be representative of the gas-surface reactions that occur in an actual hypersonic flight environment. However, bombardment of a surface with hyperthermal atoms that can lead to both thermal and non-thermal interactions might result in ablation chemistry that is not necessarily

* Corresponding author.
E-mail address: tminton@montana.edu (T.K. Minton).

https://doi.org/10.1016/j.carbon.2020.05.076
0008-6223/

representative of what occurs in the flight environment. An additional complication of Eley-Rideal reactions or non-thermal inelastic scattering is that the functional form of the product angular distribution is generally not known, especially for scattering outside the plane defined by the incident molecular beam and the surface normal, which makes the determination of relative fluxes of various products very difficult unless their angular distributions are measured. Although angular distributions may be measured, this becomes impractical if angular distributions must be measured with many surface temperatures (T_s) in order to derive relative fluxes as a function of T_s. The pulsed nature of the hyperthermal beams employed in the earlier studies adds another challenge to the determination of relative flux, because the flux-weighted integration of the products that exit the surface as a function of time after the incident pulse strikes the surface is uncertain, both because the time at which a product exits the surface is not well-known and because a slowly-decaying signal might be lost in the noise and missed. In the limit where surface chemical processes are occurring on a long time scale, product signals are not correlated with the incident beam pulse and cannot be discerned easily from the steady-state background. In fact, differences in the interpretation of the data resulting from the uncertainty in integrated flux have led to qualitative differences in the temperature-dependent CO flux in the two oxygen-carbon finite rate models that have been proposed [8–10]. Finally, strong signals from non-thermal scattering processes tend to overlap in time with signals from thermally-desorbed products, requiring a deconvolution procedure that is not necessarily unique and adding further uncertainty to the determination of the flux of the thermally-desorbed products.

In order to verify the mechanistic insight gained from the earlier molecular beam studies under conditions more relevant to hypersonic flight and to obtain accurate temperature-dependent reaction efficiencies for these conditions, we have conducted new molecular beam-surface scattering experiments with lower-energy (~0.35 eV) continuous beams containing atomic oxygen or nitrogen. With the lower incident energy, non-thermal processes are negligible and the product angular distributions are all essentially the same regardless of incident angle and T_s. In addition, the products exit the surface continuously, so the determination of product flux is not dependent on the time at which the products were formed on the surface. Thus, the relative product fluxes can be measured in a more straightforward manner than in the prior studies with hyperthermal incident beams. Furthermore, the incident O- or N-atom flux in the new experiments is up to three orders of magnitude higher than the fluxes used in the earlier studies with the hyperthermal pulsed beams, potentially amplifying coverage-dependent processes that were relatively important in the earlier studies. The new experiments corroborate the thermal gas-surface interaction mechanisms inferred from the earlier studies, and they reveal the atom-atom recombination reactions that were not clearly observed in those studies. Of particular relevance to the development of air-carbon ablation models, the new results provide quantitative data under relevant conditions on the relative efficiencies with which the various gas-surface interactions occur.

2. Experimental methods

The experiments used a molecular beam-surface scattering technique that is similar to the technique used earlier to investigate the oxidation and nitridation reactions on a carbon surface with hyperthermal beams of O or N atoms [5–7]. However, the experiments described herein used a different apparatus in Perugia, Italy [13–17], which is fitted with a high-pressure radio frequency (RF) discharge source [18,19] for producing a continuous supersonic beam containing O or N atoms with much lower velocities. A schematic diagram of the experimental setup is shown in Fig. 1. Not shown in Fig. 1 are ion deflector plates to prevent residual ions in the incident beam from striking the sample and a water-cooled copper surface to protect the chopper wheel from radiative heating from the hot sample. The continuous beam was directed at a heated sample surface, and the products that scattered from the surface were detected with a rotatable mass spectrometer. The rotation axis of the mass spectrometer was coincident with the axis of rotation of the surface, and the surface normal was contained in the mass spectrometer rotation plane. A mechanical chopper wheel was placed in front of the detector to modulate the products that scattered continuously, in steady state, from the surface. Number density distributions, $N(t)$, of short pulses of products that passed through slots on the chopper wheel at a given angular position of the mass spectrometer were accumulated as a function of flight time from the chopper wheel to the ionizer of the mass spectrometer (a distance of 22.9 cm). These $N(t)$ distributions are commonly referred to as time-of-flight (TOF) distributions. TOF distributions may be collected at a variety of final angles, θ_f, for a given incident angle, θ_i. The surface normal defines the zero angle, and θ_i and θ_f are on opposite sides of the surface normal. In order to characterize the incident molecular beam, the mass spectrometer was aligned with the incident beam, and TOF distributions of the components of the beam were collected. Probability density distributions (proportional to scattered flux) as a function of velocity, $P(v)$, or translational energy, $P(E_T)$, may be obtained from the measured $N(t)$ distributions using the relationships, $P(v) \propto t\,N(t)$ and $P(E_T) \propto t^2\,N(t)$, respectively. The total relative flux of a particular product at a given θ_f was obtained by appropriate integration of the relevant TOF distribution, $I(\theta_f) \propto \int_{t=t_i}^{t=t_f} N(t)/t\ dt$, where I is total flux, t_i is the time at which the chopper wheel slot passes in front of the detector, and t_f is the time after which the signal has decayed to the background level.

For the present experiments, the crossed molecular beams apparatus, typically used for reactive scattering studies [13–17], was upgraded with improved pumping of the main scattering chamber, where the sample surface was located (see Fig. 1). Specifically, two magnetically suspended turbomolecular pumps (each with a pumping speed of 1850 L s^{-1}), backed by a dry roots pump (110 m^3 h^{-1}), replaced two baffled oil diffusion pumps of similar pumping capacity, in order to ensure a cleaner high vacuum. In addition, a new 3600 L s^{-1} cryopump (10 K), which replaced an older 3500 L s^{-1} cryopump (20 K), augmented the main chamber pumping capacity to ensure a base pressure of 2×10^{-7} Torr. The triply differentially pumped mass spectrometer detector (base pressure of approximately 10^{-11} Torr) features an entrance aperture of 4.3 mm × 4.3 mm for detection of scattered products and 300 μm dia. for monitoring the beam directly, a tunable electron impact ionizer, a quadrupole mass filter, and a Daly-type ion detector. The computer-controlled system for collecting TOF distributions is based on a four slot (1.2 mm wide slots) chopper, 13.5 cm diameter and spinning at 150 Hz, and a high-speed multichannel scaler operated at 1 μs dwell time.

O_2 and N_2 gases were used as precursors for the production of beams containing mixtures of either O and O_2 (hereafter referred to as the "oxygen beam") or N and N_2 (hereafter referred to as the "nitrogen beam"). For the oxygen beam, an 85 mbar mixture of 5% O_2 in He was discharged with an RF power of 300 W and then expanded through a 0.48 mm diameter water-cooled quartz nozzle. The nitrogen beam was produced with a 95 mbar mixture of 2.5% N_2 in He and discharged with an RF power of 250 W and expanded through the same nozzle. Both beams were collimated with a 0.8 mm diameter boron nitride skimmer and further collimated with a 0.4 × 0.4 mm^2 square stainless-steel aperture. The velocity distributions and mole fractions of the O and O_2 components of the

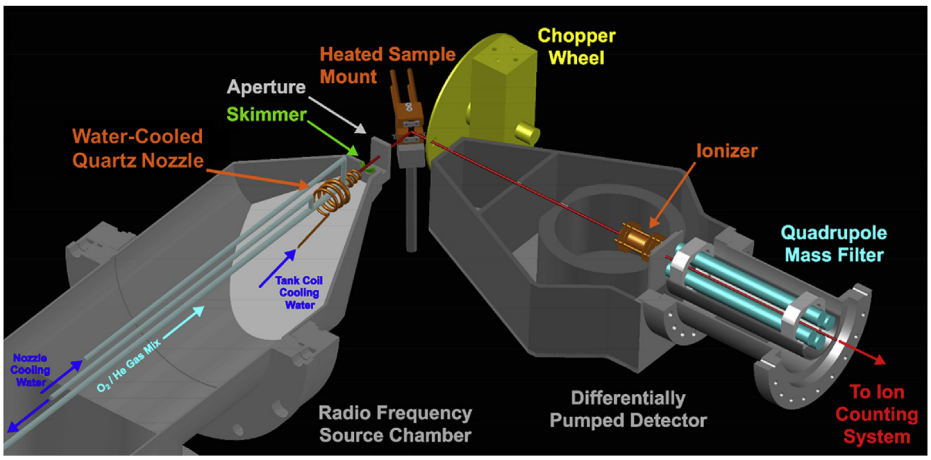

Fig. 1. Schematic diagram of the experimental setup for beam-surface scattering experiments, depicting the radio frequency molecular beam source, heated sample, mechanical chopper wheel, and rotatable mass spectrometer. The key components of the mass spectrometer are the electron-impact ionizer (electron energy of 55 eV), quadrupole mass filter, and Daly-type ion detector (not shown).[15,17] Ion deflector plates to prevent residual ions in the incident beam from striking the sample and a water-cooled copper surface to protect the chopper wheel from radiative heating from the hot sample are not shown. (A colour version of this figure can be viewed online.)

oxygen beam and the N and N_2 components of the nitrogen beam are shown in Fig. 2. The mean translational energies, $\langle E_i \rangle$, of the O and O_2 were 34.8 and 50.4 kJ mol^{-1}, respectively, with energy widths (full width half maximum, fwhm) of 25 and 45 kJ mol^{-1}, respectively. The respective mole fractions of O and O_2 were 48 and 52%. The $\langle E_i \rangle$ for N and N_2 were 35 and 47 kJ mol^{-1}, with energy widths that were nearly the same as those for the oxygen beam. The respective mole fractions of N and N_2 were 18 and 82%. The flux of O atoms in the oxygen beam was approximately eight times higher than the flux of N atoms in the nitrogen beam. Based on previous work [19], we estimate the fractions of excited O(^1D) in the oxygen beam and N(^2D) in the nitrogen beam to be 5–10% and about 25% of the O or N atoms in the beam, respectively. These excited states are not expected to play a role in the experimental results, because these states should quench very efficiently to the ground state when they interact with a surface that has no band gap. The role of excited states has been studied for species interacting with metals [20] but not vitreous carbon; however, vitreous carbon should have metallic electrons so presumably excited-state atoms that interact with vitreous carbon would behave like those on a metal.

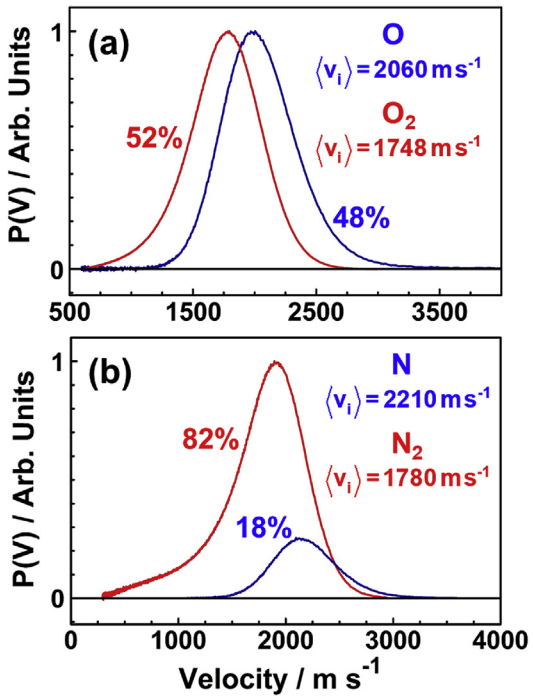

Fig. 2. Probability density distributions as a function of velocity for (a) O and O_2 in the oxygen beam and (b) N and N_2 in the nitrogen beam. The average velocities and the mole fractions of the components in each beam are indicated. (A colour version of this figure can be viewed online.)

The sample material was Grade 22 SPI-Glas vitreous carbon (Structure Probe, Inc.) [21]. Vitreous carbon is sp^2 carbon that is composed of randomly oriented graphite-like domains. The sample was 1 mm thick and was laser cut into a rectangle that was 25 mm long × 7 mm wide. The sample was placed in the vacuum chamber, with a base pressure of 2×10^{-7} Torr, and was not removed from the chamber. Thus, all the data described here were collected with one sample. The sample was heated by passing current through it in the same manner that has been described previously [5–7], and at the start of every new data collection series, the sample was first annealed at 1873 K for ~1 h or longer. We have found from numerous experiments in our lab that annealing carbon to this high temperature before data collection ensures reproducibility of the data, suggesting that all oxides or other species that might affect the oxidation or nitridation of the surface have been removed. The sample temperature was measured with an optical pyrometer that employs a heated graphite filament. The surface was assumed to be free of contamination from the vacuum environment at all temperatures used, based on earlier experiments [5,22]. During data collection, the pressure of the main scattering chamber rose to ~2×10^{-6} Torr, as a result of the increased gas load on the chamber from the molecular beam.

The experiments were conducted with the oxygen or nitrogen beam directed at the surface with $\theta_i = 60°$. With this incident angle, the beam spot had dimensions of 1.4 mm × 2.8 mm on the surface. The oxygen and nitrogen experiments were conducted in series – i.e., all data with the oxygen beam were collected first, and then data were collected with the nitrogen beam. It was determined that the most accurate comparison of O- and N-atom reactivity with a carbon surface was to use the same sample for all experiments. As implied above, before the nitrogen experiment commenced, the sample was annealed at 1873 K for >1 h in order to ensure that all oxygen was removed from the surface. The sample became

roughened by initial test experiments with the oxygen beam before the data were collected, and the data presented herein may be considered to have been collected under conditions of steady-state roughness. The reactivity of the nitrogen beam with the surface was extremely weak compared to that of the oxygen beam (see results below), so it is assumed that the surface roughness during the nitrogen experiment was essentially the same as that during the oxygen experiment. A photograph, as well as atomic force micrographs, of the sample are shown in Fig. 3. When the surface was bombarded with the oxygen beam, four product signals were observed at mass-to-charge ratios of m/z = 16, 28, 32, and 44, corresponding the products, O, CO, O_2, and CO_2, respectively. When the nitrogen beam was directed at the surface, the only signals observed were at m/z = 14, 26, and 28, corresponding to the products, N, CN, and N_2. TOF distributions for O and N were corrected for dissociative ionization of O_2 to $O^+ + O$ and for N_2 to $N^+ + N$, respectively, in the electron-impact ionizer. All TOF distributions were corrected for timing offsets associated with the chopper wheel and the ion flight time through the quadrupole mass filter. To minimize the effect of spurious signals that were not the result of beam-surface scattering events, TOF distributions for O and O_2 or N and N_2 were collected with a beam flag opened and closed, and the net TOF distributions, obtained from subtracting distributions with the beam flag closed from their respective distributions with the beam flag open, were analyzed. For experiments with both the oxygen and nitrogen beams, a tail at long flight times was observed in the TOF distributions collected at $m/z = 28$ when the sample temperatures were especially high. This signal was determined to arise from desorption of contamination from surfaces in the vacuum chamber as they were warmed by the hot sample. This "long-time" signal is thus an artifact, and it has been rejected in the determination of relative product flux at $m/z = 28$.

The temperature-dependence of the product signals was obtained by fixing the final (or detection) angle at $\theta_f = 15^\circ$ and monitoring the products as a function of surface temperature. As θ_i was fixed at 60° and θ_i and θ_f are on opposite sides of the surface normal, the total angle between the incident beam and the detection axis was 75°. The initial sample temperature was T_s = ~800 K, and T_s was increased from that point. The lowest two temperatures were estimated to be 800 K and 900 K by the dull red glow of the sample, because a reliable measurement could not be made with the pyrometer. 1073 K was the lowest temperature that could be measured accurately with the pyrometer, and from this temperature the sample was increased in 100 K increments up to a maximum of 1873 K. The maximum T_s of 1873 K was chosen, because above this temperature carbon sublimation products (e.g., C_2 and C_3) could start to be observed and their intensities rose rapidly as T_s was increased further. At each T_s, TOF distributions were collected at all relevant m/z ratios, and then the sample temperature was changed. The sample temperature was first increased in steps to 1873 K and then decreased in steps back to ~800 K; then the cycle was repeated such that four cycles of data were collected for the oxygen experiment and three cycles were collected for the nitrogen experiment, resulting in eight TOF distributions for each m/z and T_s in the oxygen experiment and six TOF distributions for each m/z and T_s in the nitrogen experiment. For the oxygen experiment, all four TOF distributions with the same m/z and T_s were added together for each of the two cases of increasing and decreasing T_s, and the summed TOF distributions were integrated, as described above, to give relative product flux. For the nitrogen experiment, all six TOF distributions with the same m/z and T_s were added together and integrated, regardless of whether T_s was increasing or decreasing. For the oxygen experiment, the four summed TOF distributions corresponded to the following numbers of "shots" through the chopper wheel: 1.2×10^6 for O, 2×10^5 for O_2, 4×10^5 for CO, and 4×10^5 for CO_2. The analogous numbers of shots for the six summed distributions in the nitrogen experiment were 3×10^5 for N, 3×10^5 for N_2, and 1.8×10^6 for CN.

Angular distributions of product flux were collected for both the oxygen and nitrogen experiments. With θ_i fixed at 60° and T_s held constant, θ_f was varied from 15° to 75° in 10° degree increments, for two cycles of increasing and decreasing angle, until four TOF

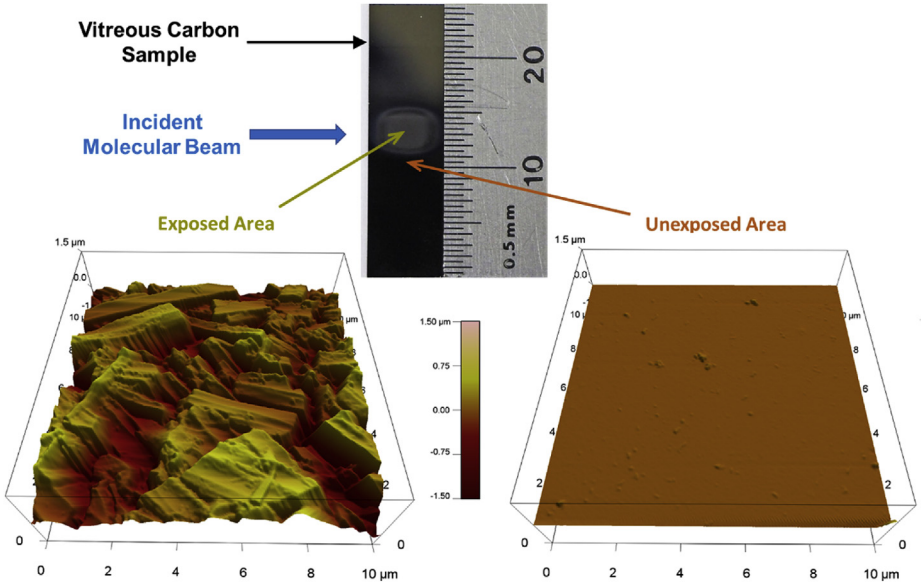

Fig. 3. Photograph of vitreous carbon sample that was used for the experiments with the oxygen and nitrogen beams and atomic force micrographs of representative areas of sample regions that were exposed or unexposed to the incident beams. The incident beam direction was from left to right, with the sample tilted such that the incident angle, θ_i, of the beam was 60° with respect to the surface normal (see Fig. 1). The region of the sample that became rough as a result of the exposure is larger than the nominal size of the beam on the tilted surface – approximately 1.4 mm high × 2.8 mm long – suggesting that incident atoms may have scattered from the edges of an aperture or migrated on the surface before reacting. The experiment with the oxygen beam was conducted first, and the exposed region of the sample became rough, as seen in the photo. The roughened region of the sample, as discernable by the naked eye, did not change during exposure to the nitrogen beam. (A colour version of this figure can be viewed online.)

distributions were collected for each m/z and θ_f. The TOF distributions for each m/z and θ_f were added together, and then the summed TOF distributions were integrated to give total relative flux for a given product at each θ_f. The total number of shots through the chopper wheel for the summed TOF distributions associated with each product were 1.2×10^6 for O, 2×10^5 for O_2, 4×10^5 for CO, and 4×10^5 for CO_2. Four angular distributions were obtained in the oxygen experiment, corresponding to four sample temperatures, $T_s = 800$ K, 1273 K, 1573 K, and 1873 K. One angular distribution was collected, at $T_s = 1873$ K, for the nitrogen experiment. The total number of shots for the summed TOF distributions in this experiment were 2×10^5 for N, 2×10^5 for N_2, and 4×10^5 for CN. The relative product fluxes reported herein for the angular distributions, as well as the temperature dependencies, take into account the accumulation time and the relative detection efficiency for each product.

3. Results and analysis

3.1. Oxygen experiment

Representative TOF distributions for the four products, O, O_2, CO, and CO_2, observed when the oxygen beam bombarded the surface at two temperatures are shown in Fig. 4. The O-atom TOF distributions have relatively poor signal-to-noise because of the high background in the mass spectrometer at $m/z = 16$. There is an obvious disappearance of CO_2 signal at the higher T_s, which has been observed in earlier experiments on the oxidation of carbon [5,6]. With the exception of the higher-temperature distribution for CO, all distributions could be fit to a Maxwell- Boltzmann (MB) distribution corresponding to the surface temperature within the signal-to-noise limits of the data. As mentioned above, there was a slow tail in the $m/z = 28$ TOF distributions for the experiments with both the oxygen and nitrogen beams, which we determined to be an artifact, probably from the desorption of CO, or perhaps N_2, from various surfaces in the vacuum chamber or on the sample mount as the sample temperature was raised to high temperatures. Thus, for each $m/z = 28$ TOF distribution at higher temperature, a MB distribution was fit to as large a section of the rising edge as possible without exceeding the values of the data points, and the residual (shown in blue in Fig. 4f) was taken to be signal from the artifact and was ignored. We have no evidence that any observed signals could not be described adequately by a MB distribution of product velocities corresponding to T_s. This result suggests that all products were in thermal equilibrium with the surface prior to desorbing into the vacuum at every combination of θ_f and T_s. If there were a significant probability for incident O or O_2 to scatter impulsively after one or only a few bounces before thermal equilibrium was attained, then there should be a clear signature of impulsive scattering in the TOF distributions [23,24], which there is not. Furthermore, it is expected that multiple bounces of incident O and O_2 on the exceedingly rough surface would drive these species into thermal equilibrium quickly. Therefore, while it is possible that a small fraction of impulsively scattered products struck the surface and then came into thermal equilibrium before desorbing, it is much more likely that the incident O or O_2 came into thermal equilibrium with the surface and then either desorbed or reacted. We thus assume that all observed products are the result desorption after various thermal adsorption, absorption, and reactive events have occurred on the surface.

The angular distributions of O, O_2, CO, and CO_2 are also consistent with the conclusion that all products desorbed in thermal equilibrium with the surface. Representative angular distributions for $T_s = 800$ and 1873 K are shown in Figs. 5 and 6, respectively. Every angular distribution collected at $T_s = 800$, 1273, 1573, and 1873 K can be fit with a cosine power law distribution in the form of $\cos^m(\theta_f)$, where m is in the range 1.0–1.3, with the exception of the angular distribution of CO_2 (collected only at $T_s = 800$ K), where $m \approx 1.8$. The $\cos^m(\theta_f)$ functional form is indicative of a randomized scattering angle distribution, which is a characteristic of thermal desorption [23], and a value of m that is greater than 1.0 may indicate a desorption barrier [6] or perhaps some degree of steering of the products as they desorb from a very rough surface [25–29]. Given that the $\cos^m(\theta_f)$ function is cylindrically symmetric and that the value of this function varies by less than 3% for $1.0 < m < 1.8$ at $\theta_f = 15°$, we used TOF distributions obtained at this final angle to derive the relative fluxes of the four products as a function of temperature as the sample was heated.

The temperature dependencies of the O, O_2, CO, and CO_2 fluxes are shown in Fig. 7. In general, the O-atom flux initially decreases with increasing T_s in the range 800–1273 K, and then it increases significantly with T_s above 1273 K. Hysteresis is observed in the temperature dependence of the O-atom flux above 1273 K – the O-atom signals are lower when T_s increases and higher when T_s decreases. However, this trend appears to be reversed for the lowest two temperatures, 800 and 900 K, where the scattered O-atom flux is marginally higher when T_s increases. The O_2 flux remains essentially unchanged with T_s from 800 K to at least 1073 K. At $T_s = 1273$ K and above, the O_2 flux increases with increasing surface temperature and is lower when T_s increases than when it decreases. The CO flux rises rapidly as T_s increases from 800 to 1073 K, goes through a maximum at T_s ~1173 K, and then starts to decrease gradually as T_s increases further. In contrast to the temperature-dependent O and O_2 fluxes, the CO flux is higher when T_s increases than when it decreases. In a separate experiment (data not shown) where the sample was heated quickly to 1473 K, the CO flux decreased from a value corresponding to the red curve in Fig. 7 to a constant value corresponding to the blue curve in this figure during a time of ~60 min. The CO_2 flux decreases with T_s and is essentially zero at $T_s = 1373$ K and above.

The data presented in Fig. 7 allow the calculation of the reaction efficiency for a given product. This calculation requires an assumption about the O-atom recombination probability on the surface ($O_{(s)} + O_{(s)} \rightarrow O_{2(g)}$), which we take to be zero in the range $800\ K < T_s < 1173\ K$. O_2 in the incident oxygen beam has an extremely low reactivity with the surface compared to O atoms [5,6], so we expect that essentially all the incident O_2 molecules would exit the surface through non-reactive scattering events and be detected as a constant background flux. O-atom recombination would add to the O_2 flux, and if this additional O_2 flux were significant enough, then it would be discernable from the O_2 background flux. If we assume that O-atom recombination is temperature-dependent and that the constant O_2 flux observed at $800\ K < T_s < 1173$ K is from non-reactive scattering of O_2 in the incident beam, then we can make the assumption that the O-atom recombination probability is zero in this temperature range and subtract the constant O_2 flux as an offset to the O-atom recombination signal. The remaining flux may then be taken to be the flux of O_2 from O-atom recombination. Given the large fraction of O_2 in the incident beam, the constant O_2 flux at the lower T_s range must be dominated by unreacted O_2, so the error in making this assumption is expected to be small, unless there is a significant dependence of the O_2 sticking probability on T_s. Under the assumption that the O-atom recombination probability is zero for $800\ K < T_s < 1173$ K, the results in Fig. 7 have been represented as reaction efficiencies in Fig. 8, where reaction efficiency is defined as:

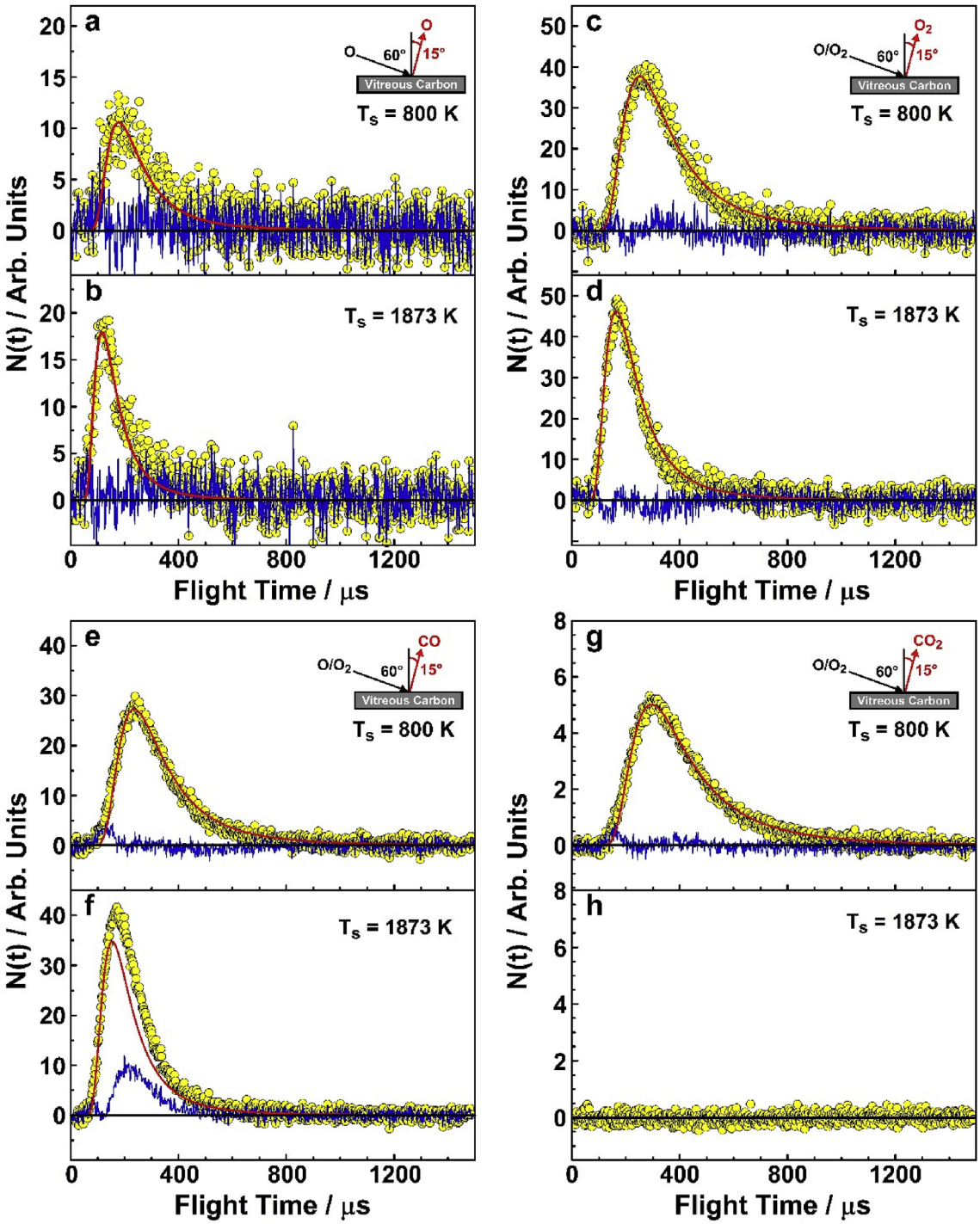

Fig. 4. Representative TOF distributions for (a,b) O, (c,d) O_2, (e,f) CO, and (g,h) CO_2 that exited the vitreous carbon surface held at 800 (top) and 1873 K (bottom) following bombardment with the oxygen beam at an incident angle, θ_i, of 60°. Time $t = 0$ μs indicates the time at which the chopper wheel slot passes in front of the detector. The yellow symbols are experimental data, which correspond to relative number density as a function of arrival time in the electron-impact ionizer of the mass spectrometer. The red lines represent Maxwell-Boltzmann (MB) distributions corresponding to the surface temperature (T_s). The blue lines represent the residual number densities not captured by the MB distributions. The residual signal for CO at longer flight times is attributed to an artifact (see text). (A colour version of this figure can be viewed online.)

$$\text{Reaction Efficiency} = \frac{\text{flux of specific product}}{\text{flux of O atoms onto surface}} = \frac{n\ f(product)}{f(O + 2O_2 + CO + 2CO_2)} \quad (1)$$

where the total flux of O atoms exiting the surface in all products is taken to be the total flux of O atoms incident onto the surface. Note that O_2 in the incident beam is not considered because its reactivity is assumed to be negligible compared to that of O atoms and the scattering of unreacted O_2 molecules is accounted for by subtracting the background O_2 signal observed in the range, 800 K < T_s < 1173 K. The factor, n, is equal to the number of O atoms

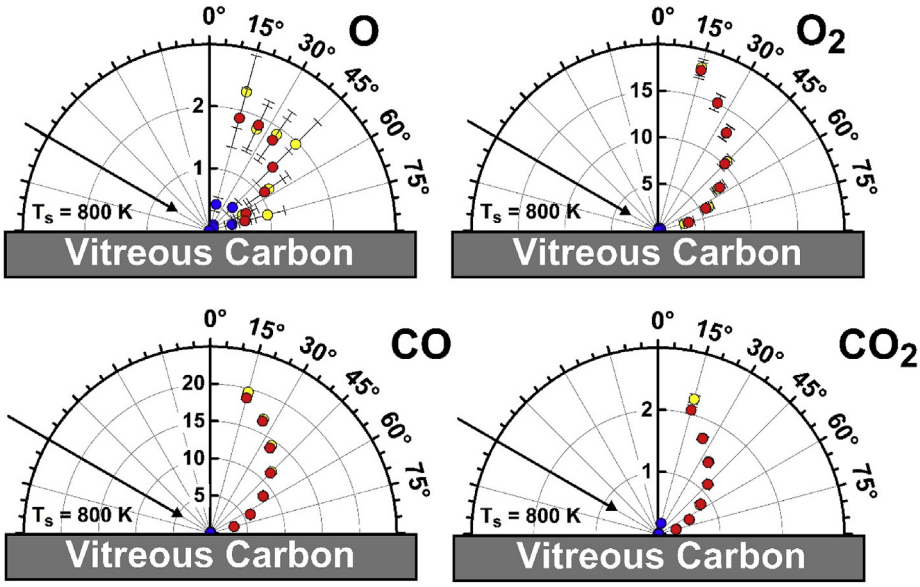

Fig. 5. Angular distributions of scattered O, O_2, CO, and CO_2 flux following bombardment of the vitreous carbon surface held at $T_s = 800$ K with the oxygen beam at $\theta_i = 60°$. The yellow symbols represent the total flux, and the red symbols represent the flux corresponding to the MB fits to the TOF data (see Fig. 4). The residual differences between the yellow and red symbols are shown as the blue symbols. Error bars indicate 95% confidence limit. (A colour version of this figure can be viewed online.)

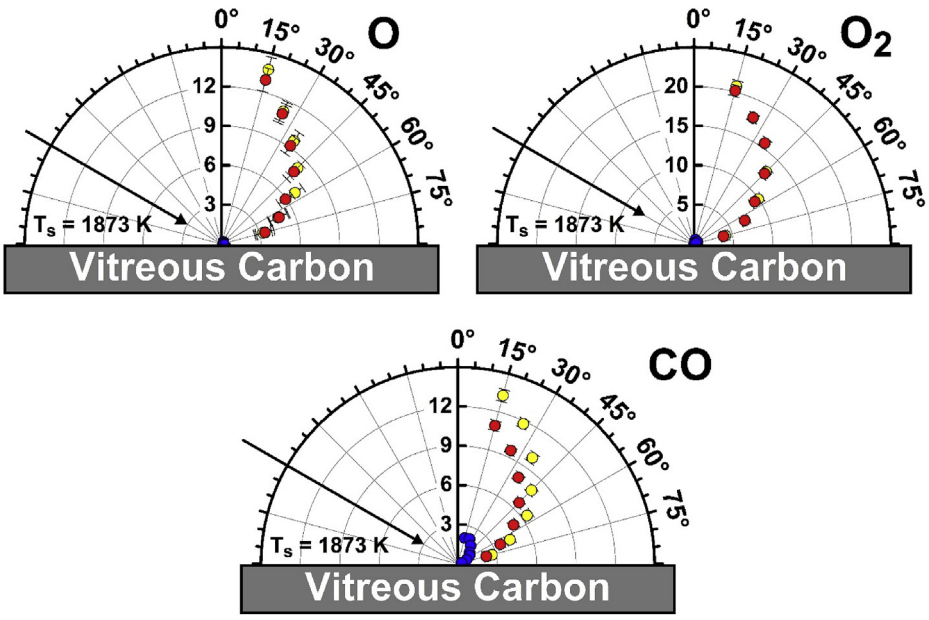

Fig. 6. Angular distributions of scattered O, O_2, and CO flux following bombardment of the vitreous carbon surface held at $T_s = 1873$ K with the oxygen beam at $\theta_i = 60°$. The yellow symbols represent the total flux, and the red symbols represent the flux corresponding to the MB fits to the TOF data (see Fig. 4). The residual differences between the yellow and red symbols are shown as the blue symbols. As mentioned in the text, the residual in the CO flux at high temperatures is an artifact, so the red symbols are assumed to represent the actual angular distribution for CO. Error bars indicate 95% confidence limit. (A colour version of this figure can be viewed online.)

contained in the given product. As an example, the use of $n = 2$ for O_2 implies that the reaction efficiency of O_2 represents the probability that an incident O atom will recombine with another O atom to become part of an O_2 molecule. Thus, the reaction efficiency is identical to the recombination coefficient, γ, which is typically defined as the fraction of particles striking a surface that recombine.

The total flux of oxygen atoms in all scattered products may be expected to be a constant function of T_s; however, we observed that the total O-atom flux was lower at lower T_s than at higher T_s. Fig. 9 shows that the total O-atom flux increased by about 30% between $T_s = 1275$ K and $T_s = 1575$ K. (The difference in measured flux at 1573 K and 1873 K is considered to be within the uncertainty of the measurement.) The reason for this increase in total O-atom flux at higher T_s is not clear, but this behavior is qualitatively similar to the result of the earlier study with the pulsed, hyperthermal incident beam [5,9]. The data in Fig. 9 were collected after the sample had been exposed to the oxygen beam for many hours at each T_s, which should have allowed a steady-state surface coverage to be reached at each T_s. Thus, effects of time-dependent coverages of O, which

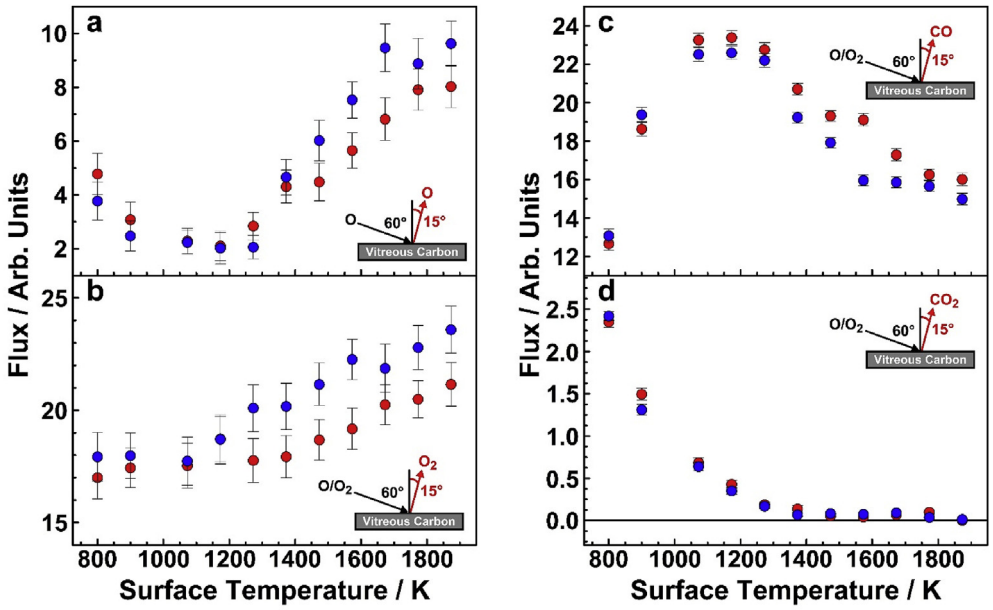

Fig. 7. Total relative flux of desorbed O, O_2, CO, CO_2 as a function of T_s with $\theta_i = 60^\circ$ and $\theta_f = 15^\circ$, following bombardment of the vitreous carbon surface with the oxygen beam. The red symbols correspond to data collected when T_s was increased, whereas the blue symbols correspond to data collected when T_s was decreased. Error bars indicate 95% confidence limit. (A colour version of this figure can be viewed online.)

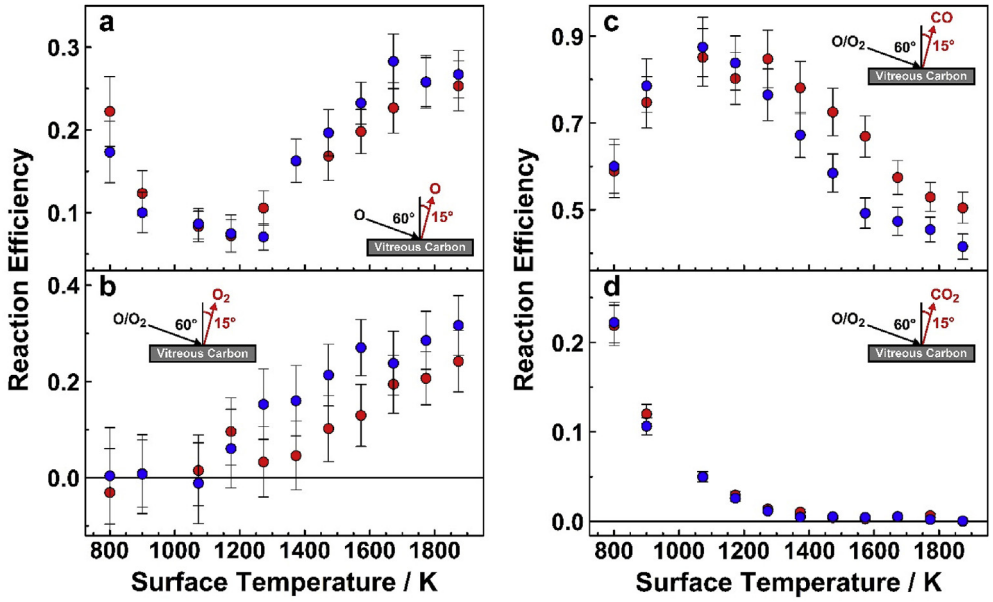

Fig. 8. Reaction efficiencies of O, O_2, CO, CO_2 as a function of T_s following bombardment of the vitreous carbon surface with the oxygen beam. The red symbols correspond to data collected when T_s was increased, whereas the blue symbols correspond to data collected when T_s was decreased. Error bars indicate 95% confidence limit. (A colour version of this figure can be viewed online.)

may be related to the T_s-dependent hysteresis in product fluxes [5,6,30], should play a minimal role in the data in Fig. 9. Although there is a slight possibility that O-containing products other than the four focus products were produced, we observed no evidence for such products in this experiment or in earlier related experiments [5,6], so it is unlikely that the increased O-atom flux at higher T_s arises from the increased desorption of an unobserved O-containing product. A possible explanation is that surface O atoms tend to migrate out of the detection area with a higher probability at lower T_s than at higher T_s. The photograph of the etched area of the surface (Fig. 3a) shows that this area is roughly twice the size of the area that was exposed to the incident beam, which is consistent with surface migration of O atoms before reaction. In addition, the desorption rate of O atoms from the surface increases rapidly as T_s rises above 1273 K (see Fig. 8a), suggesting that the residence time of O atoms on the surface may become too short for significant migration to occur at higher T_s. Thus, a larger fraction of the incident O atoms might migrate out of the detector viewing region on the surface (approximately 3 mm × 3 mm) at lower T_s than at higher T_s and lead to anomalously low signal intensities at lower T_s. However, the millimeter-scale migration of O atoms before reaction seems unlikely at temperatures of >800 K, and the enlarged area of

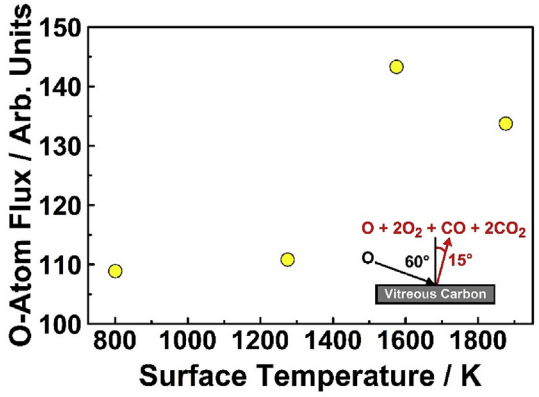

Fig. 9. Flux of O atoms exiting the surface in all products as a function of T_s, obtained by integrating angular distributions collected at $T_s = 800$ K, 1273 K, 1573 K, and 1873 K. Each point corresponds to the integral of all angular distributions collected in the range, $15° \leq \theta_f \leq 75°$. (A colour version of this figure can be viewed online.)

etching on the sample may come from scattering of O atoms from the edges of the aperture used to define the incident beam. Thus, we suggest another possibility where the incident O atoms become absorbed into the carbon bulk at lower T_s with a higher probability than at higher T_s. Depending on the lifetime of the absorbed O atoms and/or their reaction products before desorption, the fraction of incident O atoms that leave the surface in various products might appear to increase with temperature. This explanation requires that the absorbed O atoms or their products remain in the material on the time scale of hours at the lower temperatures, which may seem long. But O-atom absorption might be related to the temperature-dependent hysteresis in the O, O_2, and CO signals, which must be caused by processes that occur on the time scale of tens of minutes to hours or it would not be observed. Ultimately, we do not have definitive evidence for either of the proposed explanations for the T_s-dependent flux of O atoms that is observed in the data presented in Fig. 9. Thus, the reaction efficiencies in Fig. 8 should be considered as relative quantities that are derived for all process that lead to volatile products under the steady-state conditions that are reached on the time scale of our experimental measurement and that produce those volatile products within the detector viewing region of the surface.

3.2. Nitrogen experiment

Representative TOF distributions for the three products observed when the surface was bombarded by the nitrogen beam are shown in Fig. 10. Similar to the TOF distributions of the products observed with the oxygen beam (Fig. 4), the TOF distributions in Fig. 10 are indicative of products that desorb in thermal equilibrium with the surface. The signal at long flight times for N_2 (detected at $m/z = 28$) that cannot be fit by a MB distribution is attributed to an artifact, as discussed above. Similar to the angular distributions for the products observed with the oxygen beam, the angular distributions observed with the nitrogen beam (Fig. 11, only collected at $T_s = 1873$ K where the CN signal was large) could be fit with a $\cos^m(\theta_f)$ function with $m = 1.0$ for N and N_2 and 1.4 for CN.

Relative fluxes of the N, N_2, and CN products are shown in Fig. 12a–c. The signals for all N-containing products were identical when T_s was increased and decreased (i.e., no T_s-dependent hysteresis was observed), so all the TOF distributions and the fluxes derived from them for a given T_s were added together regardless of whether the sample was being heated or cooled. The fluxes of N and N_2 are much higher than that of CN. The N-atom flux remains fairly

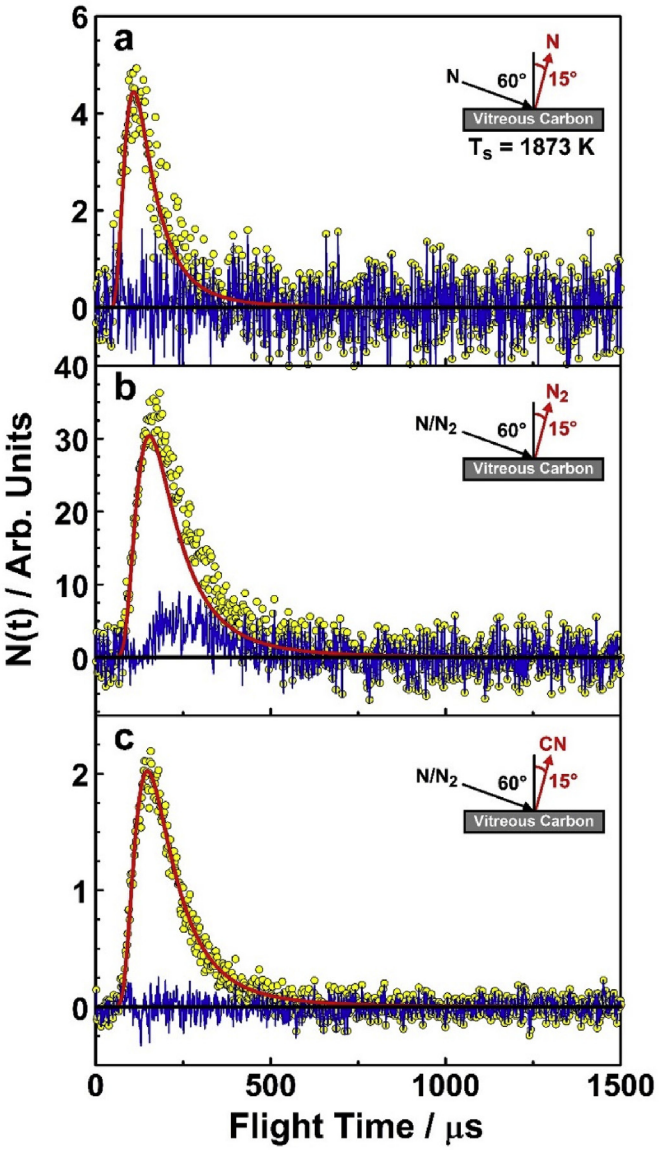

Fig. 10. Representative TOF distributions for scattered N, N_2, and CN products during bombardment of vitreous carbon at 1873 K by the nitrogen beam with $\theta_i = 60°$. Time $t = 0$ μs indicates the time at which the chopper wheel slot passes in front of the detector. The yellow symbols are proportional to the number densities of products detected in a 1 μs time interval (dwell time). The red lines represent MB distributions characterized by T_s. The blue lines represent the residual number densities not captured by the MB distributions. The residual signal for N_2 at longer flight times is attributed to an artifact (see text) (A colour version of this figure can be viewed online).

constant across the whole temperature range, while the N_2 flux rises gradually at $T_s \lesssim 1200$ K. In contrast to the relatively slowly changing fluxes of N and N_2, the flux of CN rises exponentially with T_s and may be fit well with an Arrhenius function having an activation energy of $E_a = 172$ kJ mol^{-1}. This result compares favorably with the value of 207 kJ mol^{-1}, which was reported as an upper limit in an earlier study of N-atom reactions with vitreous carbon which used a pulsed beam of hyperthermal N atoms [7]. The high flux of N_2, especially at $T_s < 1200$ K, is undoubtedly dominated by non-reactive scattering of N_2 from the incident nitrogen beam. The increase in N_2 with T_s is presumably the result of N-atom recombination. Given that the N-atom flux remains nearly constant and the CN flux is always very low, the rising N_2 flux with T_s suggests that the total flux of N atoms (as N, N_2, and CN) increases with T_s,

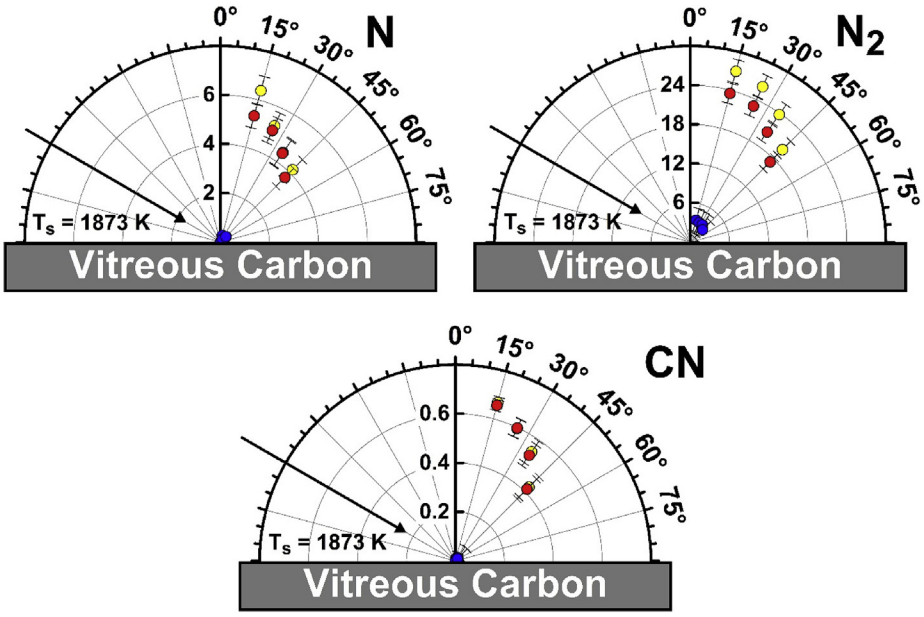

Fig. 11. Angular distributions of scattered N, N_2, and CN flux following bombardment of the vitreous carbon surface held at $T_s = 1873$ K with the nitrogen beam at $\theta_i = 60°$. Error bars indicate 95% confidence limit. (A colour version of this figure can be viewed online.)

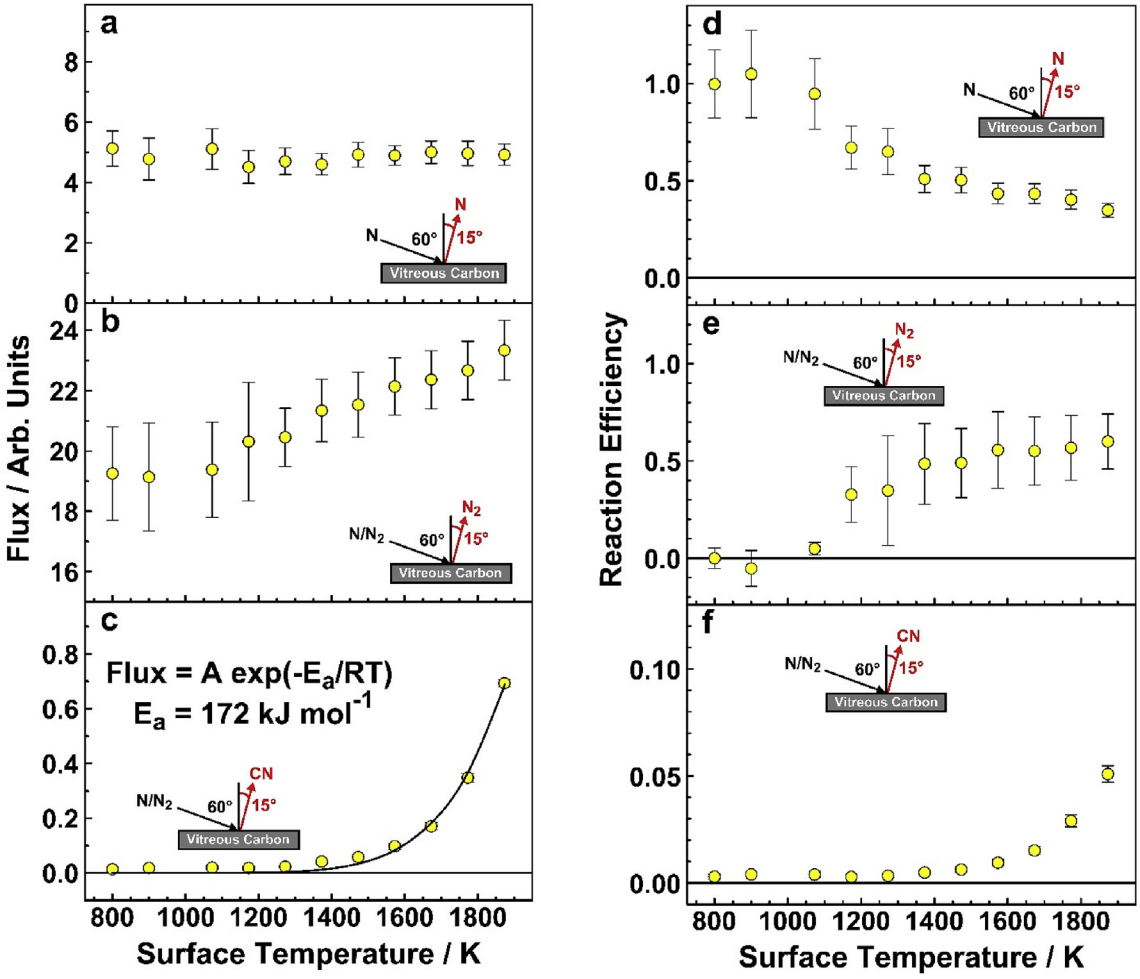

Fig. 12. (a–c) Total relative flux of desorbed N, N_2, and CN as a function of T_s with $\theta_i = 60°$ and $\theta_f = 15°$, following bombardment of the vitreous carbon surface with the nitrogen beam. (d–f) Reaction efficiencies of N, N_2, and CN as a function of T_s for $\theta_i = 60°$ and $\theta_f = 15°$. The black line in panel (c) represents an Arrhenius expression where Flux(CN) = $A \exp(-E_a/RT_s)$, with $E_a = 172$ kJ mol^{-1}. Error bars indicate 95% confidence limit. (A colour version of this figure can be viewed online.)

which would seem to violate mass balance. But as discussed above in the context of Fig. 9, it also appeared that the total O-atom flux increased with T_s, which might be attributed to reduced migration of O atoms out of the detector viewing region as the rate of various processes leading to desorbed products increases with T_s or to decreasing absorption of O atoms into the bulk carbon with increasing T_s. Analogous explanations might also be relevant to the increase in the total flux of desorbed N atoms with increasing T_s. We assume, as we did for the oxygen experiment, that nitrogen reaction efficiencies derived for a given T_s are still valid as relative efficiencies for all thermal processes that lead to volatile products during the steady-state conditions reached at each T_s in our experiment.

Reaction efficiencies for the N-containing products (Fig. 12d–f) were determined from relative product fluxes in a manner that was analogous to those obtained for the O-containing products in the oxygen experiment, where the total number of N atoms available for reaction may be represented by the denominator in the following expression for reaction efficiency:

$$\text{Reaction Efficiency} = \frac{\text{flux of specific product}}{\text{flux of N atoms onto surface}} = \frac{n\ f(product)}{f(N\ +\ 2N_2\ +\ CN)} \quad (2)$$

Similar to the flux of O_2 with bombardment by the oxygen beam, the flux of N_2 remained constant at lower temperatures and began to rise as T_s increased above 1073 K, suggesting a T_s-dependent recombination reaction that produces N_2. Thus, in analogy with the analysis of the O_2 data, the assumption was made that in the range, 800 K < T_s < 1073 K, the observed N_2 signal arose solely from N_2 molecules that were deposited onto the surface from the beam (which contained a majority fraction of N_2) and desorbed without reaction. The additional signal observed as T_s increased above 1073 K was assumed to arise from N-atom recombination reactions. Again, this assumption is valid when the sticking probability of N_2 on the surface does not vary significantly with T_s. The N-atom desorption probability relative to the total production of volatile N-containing products (Fig. 12d) drops gradually with T_s, from a value of unity at lower temperatures to ~35% at 1873 K. This decrease apparently occurs because the reaction efficiencies of N atoms to form N_2 (Fig. 12e) and CN (Fig. 12f) increase with T_s. The reaction efficiency for N_2 (i.e., N-atom recombination) rises from an assumed value of zero at 800 K < T_s < 1073 K to a plateau of roughly 50–60% between 1073 and 1573 K.

3.3. Comparison of O- and N-atom reactivity with surface carbon atoms

The ratio of CN to CO flux provides a good indication of the relative reactivity of N and O with surface carbon atoms, because the dominant product of O-atom reactions with carbon is CO and the only product of N-atom reactions with carbon is CN, and the CN product is only observed at T_s > ~1300 K where CO_2 production has dropped nearly to zero. The CN/CO flux ratio as a function of temperature is presented in Fig. 13. These data were derived from two different experiments, which used either the oxygen or nitrogen beam bombarding the vitreous carbon surface that had been annealed at high temperature (1873 K) for >1 h before data collection commenced. Thus, there were no N atoms on the surface bombarded by the oxygen beam, and there were no O atoms on the surface bombarded by the nitrogen beam. As may be seen in Fig. 13, the reactivity of N atoms with carbon is less than 5% that of O atoms

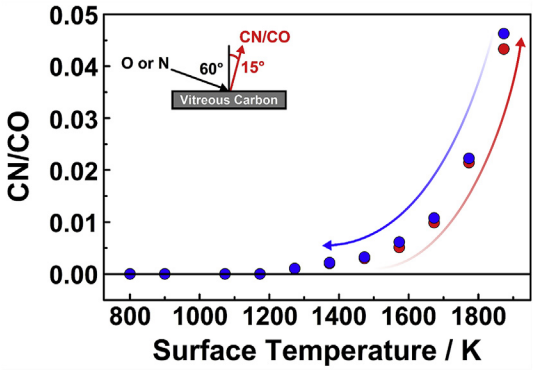

Fig. 13. Ratio of CN to CO flux as a function of T_s, for $\theta_i = 60°$ and $\theta_f = 15°$. The CN flux was derived from an experiment in which the nitrogen beam was directed at a pure (annealed) vitreous carbon surface, and the CO flux was derived from an experiment in which the oxygen beam was directed at a pure (annealed) vitreous carbon surface. The CN and CO fluxes have been normalized to the respective incident fluxes of N and O atoms. The red symbols correspond to CO fluxes when T_s was increased, whereas the blue symbols correspond to CO fluxes when T_s was decreased; the CN flux was the same at a given T_s regardless of whether the sample was being heated or cooled. (A colour version of this figure can be viewed online.)

with carbon over the range of T_s studied. The slight decrease in the CN/CO flux ratio for increasing T_s versus decreasing T_s is the result of the higher reactivity of CO when T_s increases.

4. Discussion

The new molecular beam-surface scattering experiments reported here on the oxidation and nitridation of carbon complement our earlier studies that used a similar technique [5–7]. The earlier studies used pulsed beams of O and N atoms with velocities of ~8000 m s^{-1}, whereas the new experiments used continuous beams containing O and N atoms with much lower velocities of ~2000 m s^{-1}. In addition, the average flux of the atoms onto the surface in the new experiments was 2–3 orders of magnitude higher than the flux in the earlier studies. Specifically, we estimate that the O-atom flux in the earlier study was ~10^{14} atoms cm^{-2} s^{-1} based on Kapton erosion [31], whereas the O-atom flux in the new experiment is estimated to be 4×10^{16} atoms cm^{-2} s^{-1} based on measurements done on a similar RF discharge source in the past [18]. In the earlier experiments, the N-atom flux was approximately 1/3 of the O-atom flux, whereas in the new experiments described here the N-atom flux was about 1/8 of the O-atom flux. Indeed, the observation that the sample in the earlier experiment was hardly etched and the sample in the new experiment was severely etched (see Fig. 3) is consistent with the differences in estimated incident O-atom flux. As a result of the higher incident velocity in the earlier studies, the incident O- or N-atom translational energy was ~16 times higher than the incident energy in the new experiments. A higher incident energy might increase reactivity, if Eley-Rideal (non-thermal) reactions are important. On the other hand, a higher incident energy could reduce the reactivity if Langmuir-Hinshelwood (thermal) reactions are dominant, as a higher incident energy would be expected to increase the likelihood of inelastic scattering and therefore reduce the sticking coefficient. Given the significantly lower incident energy of the atoms in the new experiments, the fraction of incident atoms that adsorbed on the surface compared to the earlier studies should be substantially higher, making the flux of adsorbed atoms in the new experiments in comparison to that in the earlier studies even higher than estimated from the incident flux alone. Another important difference is the duty cycle of the beams. With the pulsed beam, the products are

detected as a function of time after the pulse strikes the surface, and the arrival time distribution in the detector depends both on the velocity distribution of the products and the residence time of incident atoms or reaction products on the surface. While such data can add insight into the reaction mechanisms, a long residence time makes the determination of flux inaccurate, because the time at which the product leaves the surface becomes uncertain (making the number density to flux conversion uncertain) and slow product formation from the surface might be indistinguishable from detector background, especially if the noise level is significant. In a beam-surface scattering experiment with a continuous beam, all products are detected regardless of when they were formed on the surface. Thus, even though mechanistic information is lost, the determination of relative product fluxes under steady-state exposure conditions is more accurate.

Despite the significant differences between the new experiments and earlier studies, the results are remarkably similar. The reason for the similarity is that the important reactions occur in thermal equilibrium with the surface, so the incident beam acts mainly as a supply of reactive atoms to the surface. Indeed, the oxidation and nitridation products exhibit the signatures of thermal desorption: Maxwell-Boltzmann distributions of exit velocities and angular distributions with maxima near the surface normal ($\theta_f = 0°$). The flux of thermally desorbed CO increases, goes through a maximum, and then decreases as the temperature is increased. The flux of thermally desorbed CO_2 is relatively low compared to CO, and it decreases rapidly as the surface temperature increases and becomes negligible above ~1200 K. In contrast to the apparent non-Arrhenius dependencies of CO and CO_2 flux on T_s, the only observed nitridation reaction product, CN, did exhibit an Arrhenius temperature dependence, and the activation energy was found to be fairly high (172 kJ mol^{-1}), which is evidently related to the low reactivity of N with the carbon surface. In both the new experiment and in earlier studies, all products from O-atom bombardment exhibit a temperature-dependent hysteresis, where the product flux with increasing T_s is different from that with decreasing T_s. Conversely, no product from N-atom bombardment showed a T_s-dependent hysteresis. The results with the oxygen beam are consistent with the following picture: O atoms stick and react with the surface (or the near-surface region) at lower T_s, and as T_s increases the reactivity to produce CO increases. Meanwhile, the reactions that lead to CO_2 become less likely with increasing T_s because the extra O atoms needed to form CO_2 leave the surface in the form of O and CO. As T_s increases even further, the flux of CO decreases because the increasing desorption of O atoms reduces the surface coverage to the point where the number of O atoms available for reaction is significantly reduced. The reduced oxygen coverage results in increased reaction barriers and endothermicities [32], further reducing the reaction probability to produce CO. When T_s starts relatively low, the surface coverage is high (and perhaps extends into the bulk), so the reactivity to produce CO is higher and the flux of desorbed O is therefore lower. When T_s decreases from a high value, the surface coverage starts relatively low, so the reactivity to produce CO is lower and the desorption probability of O is higher. The T_s-dependent surface coverage of O may thus be related to the apparent non-Arrhenius behavior and the T_s-dependent hysteresis. The fact that the hysteresis is observed even in the new experiment with the relatively high-flux continuous beam suggests that the complex processes on the surface that eventually lead to the observed products may occur over tens of minutes or more. Nevertheless, it is clear that the hysteresis is less pronounced in the new experiment, which uses a higher flux of O atoms than the earlier studies, bolstering the conclusion that it is the result of a T_s-dependence of oxygen uptake onto the surface and perhaps even into the bulk carbon. The insight into the O-atom reaction mechanisms benefits greatly from prior theoretical work (discussed in detail in Ref. [5]); however, such a body of theory does not exist for N-atom reactions with carbon. Therefore, the details of the N-atom reaction mechanisms remain unclear. The fact that the temperature-dependent CN flux may be fit well with an Arrhenius function suggests that surface coverage of N might not be limiting the reaction rate at high temperatures, as the surface coverage of O does for the oxidation reaction to produce CO. In order to react in thermal equilibrium, N atoms would need to chemisorb to the surface. A high barrier to chemisorption might explain the observed Arrhenius dependence. On the other hand, the breaking of a C—CN bond on the surface to form the CN radical might be the source of the high activation energy, especially if the dangling bond cannot easily be stabilized, as is the case for O-atom stabilization of the dangling bonds when CO is formed on an O-covered surface [32]. Even though mechanistic details must await future theoretical studies of N-atom reactions on a hot carbon surface, we argue below that the activated release of the CN radical from the surface is the likely reason for the high activation energy for the formation of CN.

While it is gratifying that experiments with pulsed and continuous beams with significantly different incident energies provide qualitatively similar results, the new experiments have yielded reaction efficiencies for all observed products that were difficult or impossible to obtain from the earlier experiments. Admittedly, the new data were collected under rather ill-defined conditions of incident flux, surface chemistry, and surface roughness; nevertheless, because the surface was undoubtedly highly defected and oxygen- or nitrogen-covered it is a reasonable representation of a carbon surface in a hypersonic flow. In addition, the experiments were conducted with continuous and relatively high-flux beams with velocities of ~2000 m s^{-1}, making them more relevant to gas-surface interactions on hypersonic vehicles. Thus, the quantitative data reported here provide benchmarks for models of hypersonic ablation.

A particular feature of the new data is the observation of atom-atom recombination efficiencies, of which these experiments provide a relatively direct measure. The recombination efficiency (or coefficient) for O atoms on amorphous carbon at a temperature that was apparently near ambient has been reported to be $\gamma = (1.3 \pm 0.3) \times 10^{-3}$ [33], which is roughly two orders of magnitude lower than the values we report at $T_s > 1200$ K. This result thus supports our taking the value of the recombination efficiency to be zero at lower temperatures. Further support comes from temperature-programmed desorption studies that focused on the thermal decomposition of graphite oxide below 1000 K, where O_2 was not observed [34,35]. Additional theoretical and XPS studies suggest that recombination of O atoms competes with gasification reactions to produce CO and CO_2 on a non-defected graphite surface in the same temperature range and that increasing lattice damage favors the gasification reactions [36,37]. These results also suggest that O-atom recombination may indeed not be significant on our highly-defected surface in the lower-temperature range of our experiment. If the sticking coefficient of O_2 (from the incident beam) had a significant temperature dependence, then the interpretation of the increasing O_2 signal with T_s might be erroneous. Given the fact that the fluxes of O and O_2 in the incident beam are roughly equal, the temperature-dependent sticking coefficient of O_2 would not be relevant to the interpretation of the current data unless it became greater than a few percent of the sticking coefficient of O over the temperature range studied. The sticking coefficients of O and O_2 on the experimental surface are unknown; nevertheless, some inference into the relative reactivities of these two species may be drawn from previously published work. The reactivity of hyperthermal (~5 eV) O atoms with carbon on a

roughened HOPG surface at $T_s = 493$ K has been reported to be ~10% [38]. Although it is possible that the high incident energy might have contributed to this high reactivity, the surface roughness would be expected to promote multiple scattering events at the surface that would drive the atoms into thermal equilibrium before they could react. Furthermore, earlier work in our laboratory suggests that the carbon gasification reactions that lead to CO and CO_2 tend to occur in thermal equilibrium. Therefore, the carbon-removal reactivity of ~10% might also apply to incident O atoms with lower incident energy. As has also been shown previously (and in the work reported here) the carbon-removal reactivity increases dramatically with increasing T_s, so for $T_s > 1000$ K O-atom reactivity with carbon on a defected graphite surface might be much higher than 10%. The reactivity of O_2 to remove carbon atoms on highly-defected HOPG is always less than 0.05% in the range $1275 < T_s < 1475$ K with 0.4 and 0.7 eV O_2 molecules, with the reactivity at 1275 K being at least an order of magnitude less than 0.05% [39]. Presumably, any O_2 molecules that do not react will desorb as O_2, so the effect of reactions of O_2 with the surface in our experiment would be expected to be well below the noise level across the whole temperature range. Given the extremely weak reactivity of O_2 compared to O and the evidence from earlier studies suggesting that O-atom recombination is not expected to be significant on highly-defected or amorphous carbon surfaces at temperatures below 1000 K, we conclude that the temperature-dependent rise in the O_2 signal above 1200 K is the result of O-atom recombination reactions on the surface that produce O_2.

Although the experiments suggest a significant O-atom recombination efficiency at higher temperatures, there is no theoretical or spectroscopic support to aid the interpretation of this result. It is clear that the O-atom recombination efficiency increases with increasing T_s. This trend may be related to the increase in O-atom desorption with temperature, which suggests that O-atom mobility on the surface (or even beneath the surface) becomes more facile. In addition, there is a T_s-dependent hysteresis in the recombination efficiency that indicates a higher recombination probability with reduced surface O coverage – i.e., when T_s decreases from a high temperature after desorption of O atoms has occurred. The recombination of O atoms competes with the desorption of O atoms as well as the reaction of O atoms to produce CO. Thus, the seemingly counterintuitive result that the O-atom recombination efficiency increases when the surface coverage of O is reduced may be explained by the increased reactivity to produce CO when the surface coverage is higher [5,6]. Competition with increased O-atom desorption at higher temperatures will also presumably limit the O–O recombination probability.

The N_2 reaction efficiency as a function of temperature is qualitatively similar to that for O_2, with a pronounced increase as T_s rises above 1200 K. We expect N_2 molecules to have only physisorption interactions with the surface, so we made the assumption that scattered N_2 (present in a high mole fraction in the incident beam) should form a constant background signal at all surface temperatures, as was assumed for O_2 in the experiment with the oxygen beam. As little is known about the interactions of N atoms with a carbon surface, we assume they may chemisorb at under-coordinated (defect) sites on the surface or absorb into the bulk, after which they may recombine, probably through an activated process in analogy with O–O recombination [37], to produce N_2. The observation that the scattered N_2 flux rises significantly above $T_s \approx 1200$ K is consistent with its formation through an activated process. Therefore, we also assume that the flux of N_2 from N-atom recombination is small (i.e., within the signal-to-noise limits of the data) at $T_s < 1200$ K. This assumption is further supported by the ratio between the N_2 and N-atom fluxes at $T_s < 1000$ K (Fig. 12a and b), which is, within the uncertainty of the data, essentially the same as the ratio of N_2 and N-atom fluxes in the incident beam (Fig. 2). Thus, the reactivity of the surface to both N_2 and N at lower surface temperatures must be fairly low. Given the assumptions of constant background signal from N_2 in the beam at all T_s and a negligible N-atom recombination efficiency below $T_s = 1100$ K, we subtracted the N_2 flux at T_s below this value before analyzing the data collected with the nitrogen beam. The result is a lower limit to the T_s-dependent N-atom recombination efficiency that rises from essentially zero at $T_s < 1100$ K to >0.50 at higher temperatures (Fig. 12b). The probability that an incident N atom will react with the surface to produce CN becomes about 10% of the probability that an N atom will recombine with another N atom at the highest T_s used in the experiment. The increasing reactivity with carbon may limit N–N recombination at high T_s. In addition, desorption of N atoms at high T_s could also limit the N–N recombination efficiency. The N-atom recombination efficiency on carbon at high temperatures has been investigated previously in plasma environments, as summarized by Lutz [40]. Although there is significant uncertainty in the reported values, they tend to be lower than those seen in Fig. 12e. The most recent N-atom recombination efficiency, reported by Lutz for $T_s = 1600$ K, is $\gamma = 0.147$, which is only about 1/3 of our result at the same T_s. It is possible that the recombination efficiency depends sensitively on the nature of the carbon surface. However, our experiment used a vitreous carbon surface that had been significantly etched, so it was highly defected sp^2 carbon and may be similar to the carbon used in the plasma torch facility for the measurements reported by Lutz. A key difference in the experiments is the incident N-atom flux, which was undoubtedly higher in the plasma torch and might have led to surface saturation such that a larger fraction of incident N atoms scattered away without adsorbing and recombining on the surface.

The assumption that the recombination efficiencies are zero at $T_s \lesssim 1200$ K would imply that the reported recombination efficiencies are lower limits, which would then imply that the reaction efficiencies for the other products besides O_2 and N_2 are upper limits. On the other hand, the total desorbed flux of O atoms in the oxygen experiment or N atoms in the nitrogen experiment increases with T_s, suggesting the possibility that not all reaction pathways are taken into account in the calculation of the reaction efficiencies, which assumes that the total flux of O or N atoms desorbing from the surface is proportional to the total flux of incident O or N atoms, respectively. The reason for the T_s-dependence of the total reactive-atom flux is not clear. As mentioned above, a decrease in the fraction of reactive atoms that migrate out of the detector viewing region with increasing T_s is a possible explanation for the increase in the number of those atoms in the observed products as T_s increases. Assuming the observed processes are representative of all the thermal processes occurring on the surface within and outside the detector viewing region at the same T_s, then the derived reaction efficiencies should be valid at all T_s even if the T_s-dependent migration of atoms does not allow the total desorbed reactive-atom flux in a given solid angle to be conserved. Another possible explanation is decreasing absorption of O or N atoms into the carbon bulk with increasing T_s. If T_s-dependent sequestration of incident reactive atoms in the bulk is important, then the calculated reaction efficiencies for the observed volatile products would be too high because they would not be accounting for all the incident reactive-atom flux. This error would be expected to be greatest at lower T_s and may not be relevant at higher T_s when absorption into the bulk becomes improbable. Another potential source of error in the calculation of reaction efficiencies is in how we accounted for the signal at long times (i.e., the "artifact") in the TOF distributions at $m/z = 28$, which could lead to an overestimation of CO and N_2 product flux at $T_s > 1200$ K. Indeed, our approach to the analysis of the $m/z = 28$

TOF distributions is to find the upper limit for the "real" flux of CO or N_2 at higher T_s. Thus, it is possible that the reaction efficiencies at $T_s \gtrsim 1200$ K for CO in Fig. 8c and for N_2 in Fig. 12e are overestimated. The overestimation of the reaction efficiency for CO could mean that the reported O-atom recombination efficiencies are too low; however, an error associated with the assumption of a recombination efficiency of zero at $T_s \lesssim 1200$ K would lead to underestimated O-atom recombination efficiencies. Likewise, if accounting for the artifact in the analysis of the N_2 data leads to an overestimation of the N-atom recombination efficiencies, this would counteract the potential error associated with the assumption of an N-atom recombination efficiency of zero at $T_s \lesssim 1200$ K which would result in its underestimation. While we have endeavored to derive as accurate results as possible from our data, it is difficult ultimately to quantify the net effects of all the errors. Nevertheless, the data do support significant O- and N-atom recombination probabilities on a carbon surface, especially at $T_s \gtrsim 1400$ K, where the possible sequestration of reactive atoms in the bulk would be minimal and the other errors are potentially cancelling. The detection of all products in the molecular beam experiments and the determination of their reaction efficiencies with appropriate consideration of their uncertainties should make the data reported here useful for the development of a gas-surface-interaction model that can be scaled to higher flux.

The reactivity of N atoms with the carbon surface is much lower than the reactivity of O atoms, as evidenced by the flux ratio of CN to CO in Fig. 13. This ratio rises especially rapidly at higher temperatures, because the flux of CO is decreasing when the flux of CN is increasing. Still, the reactivity of N does not rise above ~5% of the reactivity of O atoms at the highest T_s of 1873 K. The lower reactivity of N with carbon compared to that of O atoms is consistent with the higher recombination efficiency of N atoms versus O atoms. The fact that the T_s-dependent flux of CN may be fit with an Arrhenius function suggests that competition between reaction and N-atom loss from the surface (through desorption of N or recombination to form N_2) does not affect the rate of CN production from the surface. If surface coverage of N were closely tied to the formation of CN, as O coverage is tied to the production of CO, then the T_s dependence would not be expected to fit the simple Arrhenius form. The apparent lack of a surface coverage dependence on the production of CN, with the incident N-atom flux in this experiment and with the orders-of-magnitude lower flux used in our earlier study [7], is consistent with a high-activation-energy step, such as chemisorption of N or cleavage of a C–CN bond on the surface. Assuming that N atoms must chemisorb before they can recombine, the observation of N–N recombination at much lower surface temperatures than formation of CN suggests that chemisorption of N might not be the rate limiting step in the formation of CN. Furthermore, even though the thermochemistry is not known for an N-covered carbon surface with many undercoordinated sites, the reaction of N with carbon to form surface-bound CN would be expected to be exothermic and the desorption of a CN radical would be expected to be endothermic. Thus, it seems most likely that a high barrier to desorption of CN from the surface limits the rate of its formation. The endothermicity of the desorption might thus be the main reason for the high activation energy that was observed. An understanding of the observed scattering behavior of N atoms on a high-temperature carbon surface would benefit greatly from theoretical calculations, as has the understanding of O-atom interactions on carbon.

5. Conclusion

The reactions of atomic oxygen and nitrogen on a high-temperature carbon surface have been re-examined with the use of molecular beam-surface scattering experiments that employed continuous beams. The continuous bombardment, modest incident velocities (~2000 m s^{-1}), relatively high flux (between 10^{16} and 10^{17} atoms cm^{-2} s^{-1}), and roughened and disordered surface make the exposure conditions closer to those experienced by leading-edge surfaces during hypersonic flight than were the conditions used in the earlier studies with pulsed hyperthermal beams [5–7]. In the new experiments, the scattering dynamics suggest that all products desorb in thermal equilibrium with the surface. While the qualitative conclusions have not changed, the new experiments provide quantitative information on the temperature-dependent scattering efficiencies of the reactive and non-reactive pathways, including O–O and N–N recombination that were not obtainable in the earlier studies. In addition, the activation energy for N-atom reactions with carbon to produce CN has been determined with more accuracy (172 kJ mol^{-1}) and the relative reactivity of O and N atoms on a carbon surface has shown that the N-atom reactivity is less than five percent of the reactivity O atoms at surface temperatures below 1900 K. The new quantitative results are expected to be useful for the construction of air-carbon ablation models relevant to hypersonic flight.

Declaration of competing interest

The authors declare that they have no known competing financial interests or personal relationships that could have appeared to influence the work reported in this paper.

CRediT authorship contribution statement

Vanessa J. Murray: Methodology, Investigation, Formal analysis, Data curation, Visualization. **Pedro Recio:** Investigation. **Adriana Caracciolo:** Investigation. **Chloe Miossec:** Investigation. **Nadia Balucani:** Resources, Supervision, Funding acquisition. **Piergiorgio Casavecchia:** Resources, Supervision, Methodology, Validation, Investigation, Writing - review & editing. **Timothy K. Minton:** Conceptualization, Methodology, Validation, Resources, Writing - original draft, Writing - review & editing, Visualization, Supervision, Project administration, Funding acquisition.

Acknowledgements

This work was supported by the U.S. Air Force office of Scientific Research: FA 9550-17-0057. P. R., A. C., C. M., N. B, and P. C. acknowledge financial support by the "Universita degli Studi di Perugia" ("Fondo Ricerca di Base 2017"), and Italian MIUR and Universita degli Studi di Perugia within the program "Department of Excellence – 2018–2022 – project AMIS". The authors are grateful to Profs. Tom Schwartzentruber and Scott Anderson for many helpful discussions.

References

[1] S.V. Zhluktov, T. Abe, Viscous shock-layer simulation of airflow past ablating blunt body with carbon surface, J. Thermophys. Heat Tran. 13 (1999) 50–59.
[2] M. MacLean, J. Marschall, D. Driver, Finite-Rate Surface Chemistry Model, II: Coupling to Viscous Navier-Stokes Code, 42nd AIAA Thermophysics Conference, Honolulu, HI, 27-30 June 2011. AIAA Paper No. 2011-3784.
[3] C.R. Alba, R.B. Greendyke, S.W. Lewis, R.G. Morgan, T.J. McIntyre, Numerical modeling of Earth reentry flow with surface ablation, J. Spacecraft Rockets 53 (2016) 84–97.
[4] C.R. Alba, R.B. Greendyke, J. Marschall, Development of a nonequilibrium finite-rate ablation model for radiating earth reentry flows, J. Spacecraft Rockets 53 (2016) 98–120.
[5] V.J. Murray, B.C. Marshall, P.J. Woodburn, T.K. Minton, Inelastic and reactive scattering dynamics of hyperthermal O and O_2 on hot vitreous carbon surfaces, J. Phys. Chem. C 119 (2015) 14780–14796.
[6] V.J. Murray, E.J. Smoll, T.K. Minton, Dynamics of graphite oxidation at high

temperature, J. Phys. Chem. C 122 (2018) 6602–6617.
[7] V.J. Murray, T.K. Minton, Gas-surface interactions of atomic nitrogen with vitreous carbon, Carbon 150 (2019) 85–92.
[8] S. Poovathingal, T.E. Schwartzentruber, V.J. Murray, T.K. Minton, G.V. Candler, Finite-rate oxidation model for carbon surfaces from molecular beam experiments, AIAA J. 55 (2017) 1644–1658.
[9] K. Swaminathan-Gopalan, A. Borner, V.J. Murray, S. Poovathingal, T.K. Minton, N.N. Mansour, K.A. Stephani, Development and validation of a finite-rate model for carbon oxidation by atomic oxygen, Carbon 137 (2018) 313–332.
[10] K. Swaminathan-Gopalan, K.A. Stephani, Construction of finite rate surface chemistry models from pulsed hyperthermal beam experimental data, AIP Adv. 9 (2019), 035246.
[11] P.V. Marrone, Normal Shock Waves in Air: Equilibrium Composition and Flow Paramaters for Velocities from 26,000 to 50,000 ft/sec., CAL Report AG-1729-A-2, Cornell Aeronautical Labratory, 1962.
[12] C.E. Wittliff, J.T. Curtis, Normal shock wave paramaters in equilibrium air, Tech. Rep. CAL-111, Cornell Aeronautical Laboratory, 1961.
[13] P. Casavecchia, N. Balucani, M. Alagia, L. Cartechini, G.G. Volpi, Reactive scattering of oxygen and nitrogen atoms, Acc. Chem. Res. 32 (1999) 503–511.
[14] G. Vanuzzo, N. Balucani, F. Leonori, D. Stranges, V. Nevrly, S. Falcinelli, A. Bergeat, P. Casavecchia, Reaction dynamics of $O(^3P)$ + propyne: I. Primary products, branching ratios, and role of intersystem crossing from crossed molecular beam experiments, J. Phys. Chem. A 120 (2016) 4603–4618.
[15] P. Casavecchia, F. Leonori, N. Balucani, R. Petrucci, G. Capozza, E. Segoloni, Probing the dynamics of polyatomic multichannel elementary reactions by crossed molecular beam experiments with soft electron-ionization mass spectrometric detection, Phys. Chem. Chem. Phys. 11 (2009) 46–65.
[16] P. Casavecchia, F. Leonori, N. Balucani, Reaction dynamics of oxygen atoms with unsaturated hydrocarbons from crossed molecular beam studies: primary products, branching ratios and role of intersystem crossing, Int. Rev. Phys. Chem. 34 (2015) 161–204.
[17] A. Caracciolo, G. Vanuzzo, N. Balucani, D. Stranges, P. Casavecchia, L. Pratali Maffei, C. Cavallotti, Combined experimental and theoretical studies of the $O(^3P)$ + 1-butene reaction dynamics: primary products, branching fractions and role of intersystem crossing, J. Phys. Chem. A 123 (2019) 9934–9956.
[18] S.J. Sibener, R.J. Buss, C.Y. Ng, Y.T. Lee, Development of a supersonic $O(^3P_J)$, $O(^1D_2)$ atomic oxygen nozzle beam source, Rev. Sci. Instrum. 51 (1980) 167–182.
[19] M. Alagia, V. Aquilanti, D. Ascenzi, N. Balucani, D. Cappelletti, L. Cartechini, P. Casavecchia, F. Pirani, G. Sanchini, G.G. Volpi, Magnetic analysis of supersonic beams of atomic oxygen, nitrogen, and chlorine generated from a radio-frequency discharge, Isr. J. Chem. 37 (1997) 329–342.
[20] W. Lin, G.C. Schatz, Mechanisms of formaldehyde and C_2 formation from methylene reacting with CO_2 adsorbed on Ni(110), J. Phys. Chem. C 122 (2018) 13827–13833.
[21] V.A. Drits, C. Tchoubar, P. Klimanek, X-Ray Diffraction by Disordered Lamellar Structures. Theory and Applications to Microdivided Silicates and Carbons, Springer-Verlag, Berlin-Heidelberg-New York, 1990.
[22] K.D. Gibson, S.J. Sibener, H.P. Upadhyaya, A.L. Brunsvold, J.M. Zhang, T.K. Minton, D. Troya, Hyperthermal Ar atom scattering from a C(0001) surface, J. Chem. Phys. 128 (2008) 224708.
[23] E.J. Smoll, T.K. Minton, Scattering-angle randomization in nonthermal gas-liquid collisions, J. Phys. Chem. C 123 (2019) 22887–22896.
[24] W.A. Alexander, J.M. Zhang, V.J. Murray, G.M. Nathanson, T.K. Minton, Kinematics and dynamics of atomic-beam scattering on liquid and self-assembled monolayer surfaces, Faraday Discuss 157 (2012) 355–374.
[25] K.D. Gibson, N. Isa, S.J. Sibener, Experiments and simulations of hyperthermal Xe interacting with an ordered 1-decanethiol/Au(111) monolayer: penetration followed by high-energy, directed ejection, J. Phys. Chem. A 110 (2006) 1469–1477.
[26] U. Tasic, D. Troya, Theoretical study of the dynamics of hyperthermal collisions of Ar with a fluorinated alkanethiolate self-assembled monolayer, Phys. Chem. Chem. Phys. 10 (2008) 5776–5786.
[27] K.D. Gibson, D.R. Killelea, H.Q. Yuan, J.S. Becker, S. Pratihar, P. Manikandan, S.C. Kohale, W.L. Hase, S.J. Sibener, Scattering of high-incident-energy Kr and Xe from ice: evidence that a major channel involves penetration into the bulk, J. Phys. Chem. C 116 (2012) 14264–14273.
[28] S. Pratihar, S.C. Kohale, L. Yang, P. Manikandan, K.D. Gibson, D.R. Killelea, H. Yuan, S.J. Sibener, W.L. Hase, Chemical dynamics simulations of high energy xenon atom collisions with the {0001} surface of hexagonal ice, J. Phys. Chem. C 117 (2013) 2183–2193.
[29] U.S. Tasic, T.Y. Yan, W.L. Hase, Dynamics of energy transfer in collisions of $O(^3P)$ atoms with a 1-decanethiol self-assembled monolayer surface, J. Phys. Chem. B 110 (2006) 11863–11877.
[30] D.R. Olander, J.A. Schwarz, W. Siekhaus, R. Jones, Reactions of modulated molecular-beams with pyrolytic-graphite .1. Oxidation of basal plane, J. Chem. Phys. 57 (1972) 408–420.
[31] D.A. Buczala, A.L. Brunsvold, T.K. Minton, Erosion of Kapton H by hyperthermal atomic oxygen, J. Spacecraft Rockets 43 (2006) 421–425.
[32] T. Sun, S. Fabris, S. Baroni, Surface precursors and reaction mechanisms for the thermal reduction of graphene basal surfaces oxidized by atomic oxygen, J. Phys. Chem. C 115 (2011) 4730–4737.
[33] A. Drenik, A. Vesel, M. Mozetic, P. Panjan, Recombination of atomic oxygen and hydrogen on amorphous carbon, J. Nucl. Mater. 442 (2013) S751–S754.
[34] M.J. McAllister, J.L. Li, D.H. Adamson, H.C. Schniepp, A.A. Abdala, J. Liu, M. Herrera-Alonso, D.L. Milius, R. Car, R.K. Prud'homme, I.A. Aksay, Single sheet functionalized graphene by oxidation and thermal expansion of graphite, Chem. Mater. 19 (2007) 4396–4404.
[35] F. Barroso-Bujans, A. Alegria, J. Colmenero, Kinetic study of the graphite oxide reduction: combined structural and gravimetric experiments under isothermal and nonisothermal conditions, J. Phys. Chem. C 114 (2010) 21645–21651.
[36] R. Larciprete, S. Fabris, T. Sun, P. Lacovig, A. Baraldi, S. Lizzit, Dual path mechanism in the thermal reduction of graphene oxide, J. Am. Chem. Soc. 133 (2011) 17315–17321.
[37] R. Larciprete, P. Lacovig, S. Gardonio, A. Baraldi, S. Lizzit, Atomic oxygen on graphite: chemical characterization and thermal reduction, J. Phys. Chem. C 116 (2012) 9900–9908.
[38] T. Ngo, E.J. Snyder, W.M. Tong, R.S. Williams, M.S. Anderson, O-atom etching of graphite in low-earth-orbit, Surf. Sci. 314 (1994) L817–L822.
[39] R. Edel, T. Grabnic, B. Wiggins, S.J. Sibener, Atomically-resolved oxidative erosion and ablation of basal plane HOPG graphite using supersonic beams of O_2 with scanning tunneling microscopy visualization, J. Phys. Chem. C 122 (2018) 14706–14713.
[40] A. Lutz, Experimental Investigation and Analysis of High-Enthalpy Nitrogen Flow over Graphite, Ph.D. Thesis, University of Vermont, 2015. https://scholarworks.uvm.edu/graddis/361?utm_source=scholarworks.uvm.edu%2Fgraddis%2F361&utm_medium=PDF&utm_campaign=PDFCoverPages.